International Journal of Heat and Mass Transfer 52 (2009) 2507–2515

Contents lists available at ScienceDirect

International Journal of Heat and Mass Transfer

journal homepage: www.elsevier.com/locate/ijhmt

Fluid-particle mass transport of cupric chloride hydrolysis in a fluidized bed

Y. Haseli, G.F. Naterer *, I. Dincer

Faculty of Engineering and Applied Science, University of Ontario Institute of Technology, 2000 Simcoe Street North, Oshawa, Ontario, Canada L1H 7K4

ARTICLE INFO

Article history:
Received 5 December 2008
Received in revised form 17 December 2008
Available online 27 February 2009

Keywords:
Mass transfer
Cupric chloride
Steam
Conversion
Chemical reaction
Fluidized bed
Bed effectiveness

ABSTRACT

This paper examines the mass transport phenomena of a hydrolysis reaction involving cupric chloride particles and superheated steam in a fluidized bed, as a part of the copper–chlorine thermochemical cycle for nuclear-based hydrogen production. The Gómez-Barea method was extended and utilized for the purpose of this study. A uniform reaction model (Volumetric Model; VM) and Shrinking Core Model (SCM) were used for limiting cases of the conversion processes. Using the solution procedures developed for each case, the effects of different parameters (such as the superficial gas velocity, bed inventory, and process temperature) were investigated in terms of the conversion of $CuCl_2$ particles and steam.

1. Introduction

Unlike fossil fuels, hydrogen is a clean energy carrier that does not react to produce carbon dioxide. However, a major portion of the world's hydrogen production is dependent on fossil fuels. The predominant existing process for large-scale hydrogen production is Steam Methane Reforming (SMR), which is a carbon-based technology that emits greenhouse gases. Nuclear energy can be used for large-scale capacities of hydrogen production without greenhouse gas emissions [1,2]. Thermochemical water decomposition driven uses heat to split water into hydrogen and oxygen through a sequence of chemical reactions that form a closed internal loop, which re-cycles all chemicals on a continuous basis, without emitting any greenhouse gases [3]. Optimization of heat flows is important for high energy conversion efficiency [4]. This paper investigates mass transfer processes that occur within a particular thermochemical cycle, namely a hydrolysis reaction within a copper–chlorine (Cu–Cl) cycle [1].

Many types of thermochemical processes exist for hydrogen production. The Sulfur–Iodine (S–I) cycle (involving hydrogen sulfide, iodine–sulfur, sulfuric acid–methanol) and the Br–Ca–Fe cycle are leading examples [3]. Nomura and co-workers [5] successfully employed the Bunsen reaction ($SO_2 + I_2 + 2H_2O = H_2SO_4 + 2HI$) in the thermochemical S–I process to produce hydrogen using an electrochemical membrane reactor. H_2SO_4 and HI were concentrated in the anode side and cathode side of the reactor, respectively. Kasahara et al. [6] and Kasahara et al. [7] reported a maximum thermal efficiency of 56.8% and 55.2%, respectively, for the S–I cycle. Kasahara et al. [8] have recently carried out successfully a continuous and stable operation of a bench-scale S–I cycle. Forsberg et al. [9] utilized a molten-salt-cooled Advanced High-Temperature Reactor as a reactor concept for thermochemical production of hydrogen. In past work by Summers and Gorensek [10], two variations of sulfur cycles – the Sulfur–Iodine (S–I) and the Hybrid Sulfur – emerged as leading thermochemical cycles. The copper–chlorine (Cu–Cl) cycle has been identified by Atomic Energy of Canada Limited and the Argonne National Laboratory as one of the most promising cycles for lower temperature thermochemical production of hydrogen [11–14]. This cycle is shown in Table 1.

The purpose of this article is to examine mass transport phenomena of cupric chloride particles in a hydrolysis reaction (reaction 4 in Table 1), which takes place in a fluidized bed reactor, as part of the Cu–Cl cycle. Unfortunately, little or no experimental data of hydrodynamics and chemistry of this hydrolysis reaction is available, so this article focuses on predictive modeling of the transport phenomena. A hydrodynamic analysis of both gas and solid reactants was carried out by Haseli et al. [15] for cupric chloride particles and steam in both bench-scale and full-scale hydrolysis reactors. Hydrolysis is a complex multiphase process, involving transport phenomena of solid–gas interactions and heat transfer (Naterer [4,16]). Past studies have investigated reactive spray flows of $CuCl_2$ droplets during hydrolysis. Lin and Ponnappan [17] examined spray flows of FC-87, FC-72, methanol and water. Heat transfer from an ethanol droplet stream, injected into a

* Corresponding author.
E-mail addresses: yousef.haseli@mycampus.uoit.ca (Y. Haseli), greg.naterer@uoit.ca (G.F. Naterer), ibrahim.dincer@uoit.ca (I. Dincer).

0017-9310/$ - see front matter © 2009 Elsevier Ltd. All rights reserved.
doi:10.1016/j.ijheatmasstransfer.2008.12.024

Nomenclature

$A_{c,bed}$	bed cross-sectional area, m^2
B	stoichiometric factor of the reaction
C_{Ae}	gaseous reactant concentration in emulsion phase, mole/m^3
C_{Ab}	gaseous reactant concentration in the bubble phase, mole/m^3
C_{Ai}	inlet gaseous reactant concentration, mole/m^3
C_{Ao}	outlet gaseous reactant concentration, mole/m^3
C_{pi}	inlet solid particle concentration, mole/m^3
C_{po}	outlet solid particle concentration, mole/m^3
d_p	particle diameter, mm
Da_s	Damkohler number at reactor scale, in Eq. 11
f	function
$f_2(x_{c0},\lambda)$	function defined in Eq. 16
F_0	inlet flow rate of solids, kg/s
F_1	outlet flow rate of solids, kg/s
k_0	kinetic coefficient, 1/s
K_{be}	overall coefficient of gas interchange between bubble and emulsion, 1/s
$K_{r,e}$	kinetic coefficient, 1/s
L_f	bed height, m
M_p	molecular mass of solid reactant, kg/mol
n	order of reaction
n_{CuCl_2}	number of cupric chloride mole
n_{H_2O}	number of steam mole
N_a	concentration efficiency, in Eq. 4
NTU	Number of Transfer Units defined in Eq. 5
$r_{c,bed}$	overall rate of reaction in the bed defined in Eq. 8, kg/s
$\bar{t}$	mean residence time, s
U_o	superficial gas velocity, m/s
U_{mf}	minimum fluidized velocity, m/s
W_b	bed inventory, kg
x_c	conversion of solid reactant in a particle
x_{c0}	conversion of solid reactant in a particle at inlet condition
$x_{c,b}$	average conversion of solids in the bed
X_g	gas conversion
Y_{c0}	mass fraction of solid reactant in the feed
$Y_{c,b}$	mass fraction of solid reactant in the bed

Greek letters

α	dimensionless parameter at the reactor level, in Eq. 10
β	dimensionless excess of flow, in Eq. 6
ε_b	bed void fraction
η_{bed}	bed effectiveness
η_{ph}	inter-phase effectiveness factor, in Eq. 2
$\Theta(x_c)$	kinetic function, in Table 2
λ	dimensionless factor defined in Eq. 12
μ_g	gas viscosity, kg/m.s
φ	particle sphericity
ρ_g	gas density, kg/m^3
ρ_p	particle density, kg/m^3

thermal boundary layer along a vertical heated plate, was reported by Castanet et al. [18]. Processes of transient vaporization and burning of droplets in dense sprays were predicted numerically by Imaoka and Sirignano [19]. Effects of gas solubility on droplet vaporization of fuel sprays up to 5 MPa and 800 K were studied by Hohmann and Renz [20]. The authors developed an Eulerian/Lagrangian predictive model that included effects of droplet evaporation, gas solubility and diffusion of heat and species within the fuel droplets. In addition to diffusive mass transfer with evaporation, this article includes the effects of chemical kinetics and solid formation during the process of reactive spray drying. Electrochemical diffusion in a one-dimensional solid layer was studied by Naterer et al. [21]. This paper analyzes diffusive mass transfer with chemical reactions that yield solid particles as products.

As both cupric chloride and steam participate in the hydrolysis reaction, a Non-Catalytic Gas Solid Reaction (NCGSR) model is needed, unlike past studies that have modelled the conversion of gaseous species for a catalytic gas–solid reaction (CGSR) [22]. Physical models of Kunii and Levenspiel [23] used three reactor models, depending upon the flow regimes, for predicting the conversion of reacting gas. They developed two limiting models to describe the conversion of solid particles in a NCGSR, which are based on two extremes of behaviour: a uniform reaction model, or a shrinking core model. The calculation procedure of Kunii and Levenspiel considered a combination of different models, depending on process conditions. Due to limitations of either model, it would be beneficial to develop one single model that best describes the conversion of both gaseous and solid reactants. In a recent study by Haseli et al. [24], this model has been addressed by applying the generalized model of Gómez-Barea et al. [25] to the reaction of cupric chloride particles with steam. Due to the lack of experimental data to define the kinetics of the solid reaction, the following two models were used as limiting cases: uniform reaction model (Volumetric Model – VM), and Shrinking Core Model (SCM). Haseli et al. [24] developed a separate solution procedure for each of these. In the present paper, based on the new solution algorithms, parametric studies will be performed, in order to evaluate the effects of various parameters on fluidized bed performance, in terms of conversions of $CuCl_2$ particles and steam, inter-phase effectiveness factor and a newly developed parameter called the "bed effectiveness".

Table 1
Steps in the Cu–Cl thermochemical cycle for hydrogen production.

Step	Reaction	Temperature range, bed effectiveness can be °C
1	$2Cu(s) + 2HCl(g) \rightarrow 2CuCl(l) + H_2(g)$	430–475
2	$2CuCl(s) \rightarrow 2CuCl(aq) \rightarrow CuCl_2(aq) + Cu(s)$	3–70 (electrolysis)
3	$CuCl_2(aq) \rightarrow CuCl_2(s)$	>100
4	$2CuCl_2(s) + H_2O(g) \rightarrow CuO^{*}CuCl_2(s) + 2HCl(g)$	400
5	$CuO^{*}CuCl_2(s) \rightarrow 2CuCl(l) + 1/2°_2(g)$	500

Source: Ref. [1].

2. Problem formulation

Catalytic gas–solid reactions (CGSRs) have been widely studied and there are various models describing the conversion of a gaseous reactant in a fluidized bed reactor, where the solid particles do not participate in the reaction. These models are generally based on two-phase theory. Toomey and Johnstone [26] introduced a two-phase theory of fluidization, which assumes that all gas in excess of the minimum fluidization velocity flows through the bed as bubbles, while the emulsion stays stagnant at minimum fluidization conditions. Expansion of the two-phase models to non-catalytic gas–solid reactions (NCGSRs) is difficult, since solid particles take part in the reaction as well. In this case, the method of Kunii and Levenspiel [23] can be used for two limiting models that describe the conversion of solid particles in a NCGSR. The two models are based on two extremes of behaviour: a *uniform reaction model*, or a *shrinking core model*. The key assumption of the models

for solid conversion is that reacting solids are covered with gas of the same mean composition. In the general case, however, the mean gas-phase driving force in the bed is a variable that changes with operating conditions. Thus, the conversion of solid and the concentration of gaseous reactant leaving and staying within the bed are inter-dependent. Kunii and Levenspiel [23] dealt with this interaction by a three-step calculation procedure, which is applicable to solids of constant size or changing size, although it involves tedious and time-consuming calculations.

2.1. Model of non-catalytic gas–solid reaction (NCGSR)

This section extends a recent generalized method to analyze NCGSR by Gómez-Barea et al. [25] to predict the reactive conversion of cupric chloride particles and steam in a hydrolysis reaction. Firstly, a method for the evaluation of gas conversion was formulated by applying the two-phase theory of fluidization, in a fluidized bed catalytic reactor, in which only gas conversion is considered. In a second stage, the model was extended to account for non-catalytic reactions by incorporating a variation of particle properties and a reaction rate with conversion, as well as the distribution of the conversion of reacting particles in the bed.

Consider that gaseous reactant A at concentration C_{Ai} is fed into a fluidized bed reactor, which consists of bubble and emulsion phases. Reactant A is transferred from the bubble phase (with C_{Ab}) to the emulsion phase (with C_{Ae}) to react with particles. Fig. 1 shows the problem schematic, which follows past studies in Ref. [25]. It was assumed that a solid particle S is made up of an active reactant solid particle C, and non-reactive material D. The transport resistances are the bubble to emulsion resistance, external film resistance around the solid particle, and inter-particle resistance. The reactor contains particles that have spent different periods inside the bed, and hence they have a wide distribution of conversion. Define the gas conversion, X_g, and inter-phase effectiveness factor, η_{ph}, as

$$X_g = 1 - \frac{C_{Ao}}{C_{Ai}} \tag{1}$$

$$\eta_{ph} = \left(\frac{C_{Ae}}{C_{Ai}}\right)^n \tag{2}$$

The gas conversion can be determined by

$$X_g = \left(1 - \eta_{ph}^{1/n}\right) N_a \tag{3}$$

where n denotes the order of the reaction, and

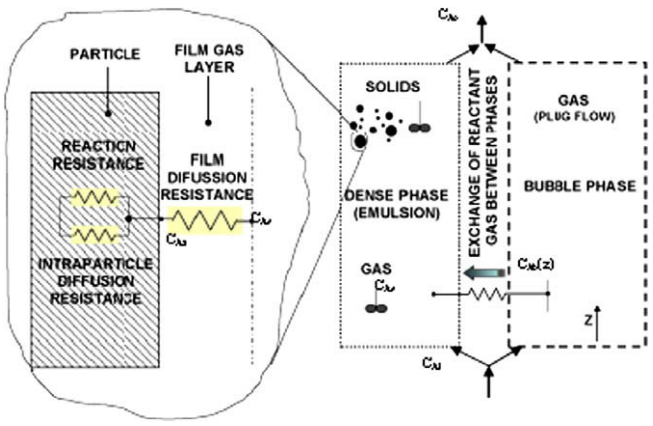

Fig. 1. Problem schematic with diffusion resistances (based on Ref. [25]).

$$N_a = \frac{C_{Ai} - C_{Ao}}{C_{Ai} - C_{Ae}} = 1 - \beta \exp\left(-\frac{NTU}{\beta}\right) \tag{4}$$

$$NTU = \frac{K_{be}\varepsilon_b}{U_o/L_f} \tag{5}$$

$$\beta = \frac{U_o - U_{mf}}{U_o} \tag{6}$$

The expression for β shows that all gas in excess of the minimum fluidization velocity was assumed to flow through the bed in the form of bubbles. The gas velocity at the minimum fluidization condition is calculated as follows.

$$U_{mf} = 0.061 g \left(\frac{\rho_p - \rho_g}{\mu_g}\right) d_p^2 \quad (\mathrm{cm/s}) \tag{7}$$

Allowance was made for the deviation from a catalytic case, considering the extent of conversion in the fluidized bed by a solid population balance. It was assumed that all fine particles are returned to the reactor and there is no carry-over. Furthermore, it was assumed that all particles enter the bed with the same conversion x_{c0}, and they are removed from the reactor at $x_{c,b}$ (average conversion of perfectly mixed particles in the bed). This approach expresses the equations in terms of the conversion, rather than time or particle size.

The overall conversion of solid particles and gaseous reactant within the bed is related through an overall mass balance for the solid particles and gaseous reactant, and the stoichiometry of the reaction, b. Thus, the following expression is derived for the gas conversion, by equating the rate of consumption of solid particles, to the rate of consumption of gaseous reactant,

$$X_g = \frac{1}{\alpha}\left(1 - \frac{Da_s}{\lambda}\right) \tag{8}$$

$$\alpha = b\frac{U_o A_{c,bed} C_{Ai} M_p}{F_0} \tag{9}$$

where Da_s and λ are dimensionless parameters that are defined as

$$Da_s = \frac{K_{r,e} W_b}{F_0} = K_{r,e}\bar{t} \tag{10}$$

$$\lambda = \frac{K_{r,e} W_b}{F_1} = \frac{K_{r,e} W_b}{F_0 - r_{c,bed}} \tag{11}$$

In Eqs. 10 and 11, $K_{r,e}$ is the kinetic coefficient as defined in Eq. 12, which accounts for the concentration of the gaseous reactant and temperature in the emulsion.

$$K_{r,e} = b\frac{M_p}{\rho_p} k_0 C_{Ae}^n \tag{12}$$

The following expression was derived to evaluate the inter-phase effectiveness factor, η_{ph}, as follows,

$$\eta_{ph} = \left[1 - \frac{1}{N_a \alpha}\left(1 - \frac{Da_s}{\lambda}\right)\right]^n \tag{13}$$

The following expression relates the conversion of gaseous reactant to that of solid particles [25]:

$$X_g = \frac{x_{c,b} - x_{c0}}{\alpha(1/Y_{c0} - x_{c0})} \tag{14}$$

In the following section, this model was applied to a specific hydrolysis reaction involving cupric chloride particles and steam.

2.2. Fluidized bed model for cupric chloride particles

Since both cupric chloride particles and steam participate in the hydrolysis reaction, it is necessary to apply a Non-Catalytic Gas–Solid Reaction (NCGSR) model to analyze the bed performance.

The following assumptions were used for analyzing the bed behavior.

- The bed consists of two regions according to two-phase theory: a bubble phase, and an emulsion phase.
- The temperature gradient within the bed reactor is negligible, so it experiences an isothermal process.
- There exists merely one reaction, namely the reaction of cupric chloride particles with superheated steam.
- The reaction takes place in the emulsion phase.
- In addition to these assumptions, for the case of the present work, the followings approximations were also used.
- Unlike the assumption of Gómez-Barea et al. [25], there exists only one type of particle that reacts with the fluidizing gas, and there is no non-reacting material, so $Y_{c0} = 1$.
- The conversion of particles at the inlet of the reactor is zero: $x_{c0} = 0$.
- The hydrolysis reaction is *first-order*.

The key aspect for determining the reactant conversion is that the ratio (Da_s/λ) is computed by combining Eqs. 11 and 12 to yield

$$\frac{Da_s}{\lambda} = 1 - \frac{r_{c,bed}}{F_0} \tag{15}$$

It can be shown that [24]

$$r_{c,bed} = F_0\left(\frac{Y_{c0}}{1 - Y_{c0}x_{c0}}\right) f_2(x_{c0}, \lambda) \tag{16}$$

Thus, combining Eqs. 15 and 16 yields

$$\frac{Da_s}{\lambda} = 1 - \left(\frac{Y_{c0}}{1 - Y_{c0}x_{c0}}\right) f_2(x_{c0}, \lambda) \tag{17}$$

Considering $Y_{c0} = 1$, $x_{c0} = 0$, the ratio (Da_s/λ) may be expressed only as a function of λ, i.e., [24]

$$\frac{Da_s}{\lambda} = 1 - f_2(\lambda) = 1 - \int_0^1 \exp\left[-\frac{\Theta(s)}{\lambda}\right] ds \tag{18}$$

Unfortunately for the hydrolysis reaction, the nature and kinetics of the reaction of cupric chloride particles is not well-known. According to Kunii and Levenspiel [23], conversion of solids can follow one of two extremes of behavior. At one extreme, the diffusion of gaseous reactant is consumed uniformly throughout the particle. This is the uniform reaction of volumetric model (VM). At the other extreme, diffusion into the reactant particle is so slow that the reaction zone is restricted to a thin front that advances from the outer surface into the particle. This model is called the shrinking core model (SCM). In this paper, these two models are treated as the limiting cases. As a result, the actual fluidized bed reactor for the hydrolysis of cupric chloride is anticipated to exist between these two kinetic model predictions. Table 2 outlines these two kinetic models for $\Theta(x_c)$. Whether the solid reaction follows VM or SCM, a separate solution procedure is needed for each kinetic model.

2.3. Fluidized bed effectiveness

Utilizing a fluidized bed in step 4 of Table 1 involves a condition under which $CuCl_2$ and steam are reacted. It is worth defining a factor that represents the effectiveness of the fluidized bed reactor. According to the stoichiometry of the reaction (see Table 1), two moles of $CuCl_2$ are reacted with one mole of steam. The best performance of the bed occurs when all three moles of reactants (two moles of $CuCl_2$ + one mole of steam) convert to products, so there is no $CuCl_2$ or steam at the exit. Thus, the "bed effectiveness" represented by η_{bed} was defined as

$$\eta_{bed} = \frac{\text{Total moles of reactants converted to products}}{\text{Total reactant moles at the inlet streams}} \tag{19}$$

$$\eta_{bed} = 1 - \frac{\text{Total non-reacted reactant moles}}{\text{Total reactant moles at the inlet streams}} \tag{20}$$

$$\eta_{bed} = 1 - \frac{\text{Total reactant moles at the outlet streams}}{\text{Total reactant moles at the inlet streams}} \tag{21}$$

In symbols, Eq. 21 can be expressed as

$$\eta_{bed} = 1 - \frac{\sum_{\text{outlet}} \text{Reactant moles}}{\sum_{\text{inlet}} \text{Reactant moles}} \tag{22}$$

For the present case of cupric chloride particles in a hydrolysis reaction,

$$\sum_{\text{outlet}} \text{Reactant moles} = (n_{CuCl_2 + n_{H_2O}})_{\text{outlet}} \tag{23}$$

$$\sum_{\text{inlet}} \text{Reactant moles} = (n_{CuCl_2 + n_{H_2O}})_{\text{inlet}} = 2 + 1 = 3 \tag{24}$$

The reactant moles at the outlet may be computed based on their conversions as shown below,

$$\frac{n_{CuCl_2|\text{outlet}}}{n_{CuCl_2|\text{inlet}}} = \frac{C_{po}}{C_{pi}} = 1 - x_{c,b} \tag{25a}$$

$$n_{CuCl_2|\text{outlet}} = n_{CuCl_2|\text{inlet}}(1 - x_{c,b}) \tag{25b}$$

and

$$\frac{n_{H_2O|\text{outlet}}}{n_{H_2O|\text{inlet}}} = \frac{C_{Ao}}{C_{Ai}} = 1 - X_g \tag{26a}$$

$$n_{H_2O|\text{outlet}} = n_{H_2O|\text{inlet}}(1 - X_g) \tag{26b}$$

Substituting Eqs. 25b and 26b into Eq. 23, and then substituting the resulting expression into Eq. 22, taking into account Eq. 24 and considering $n_{CuCl_2|\text{inlet}} = 2$ and $n_{H_2O|\text{inlet}} = 1$, yields

$$\eta_{bed} = 1 - \frac{2(1 - x_{c,b}) + 1 - X_g}{3} \tag{27}$$

Simplifying Eq. 27 gives

$$\eta_{bed} = \frac{2x_{c,b} + X_g}{3} \tag{28}$$

Hence, the bed effectiveness can be determined by a known process condition after calculating the cupric chloride particle and steam conversions within the bed reactor. In the next section, the influences of various process parameters on the bed effectiveness are presented.

Table 2
Two extremes of kinetic models for NCGSR.

Model name	VM	SCM
$\Theta(x_c)$	$-\ln(1 - x_c)$	$-3[1 - (1 - x_c)^{1/3}]$
$f_2(\lambda)$	$\frac{\lambda}{\lambda+1}$	$\lambda\left[(1 - \frac{\lambda}{3})^2 + (\frac{\lambda}{3})^2 - 2(\frac{\lambda}{3})^2 \exp(-\frac{3}{\lambda})\right]$

Source: Ref. [24].

3. Results and discussion

This section investigates the effects of various process parameters on the performance of a fluidized bed, involving hydrolysis of cupric chloride particles. Prior to the detailed simulations, validation of the newly developed models is needed. Two sets of data were obtained from past literature for comparison purposes. Both sets of data were related to a zinc roaster within an industrial (full-scale) fluidized bed. The first set was obtained by Gómez-Barea et al. [25], and the second set of data was reported by Kunii and Levenspiel [23]. The stoichiometry of the reaction is

$$O_2 + (2/3)\text{ZnS} \rightarrow (2/3)SO_2 + (2/3)\text{ZnO} \tag{29}$$

In the first example [25], zinc roasting occurred in an industrial fluidized bed with a diameter of 6.38 m at 1000 °C. The fluidizing air was fed at a velocity of 0.78 m/s. The feed rate of particles with a diameter of 60 μm was 2.48 kg/s. The bed inventory was 30,000 kg. Table 3 compares the predicted values of various parameters derived in the previous sections, with the past data. The results exhibit close agreement, particularly for the conversion values of the reactants, thus provide useful validation of the current formulation.

In the second validation case [23], zinc blend (ZnS) particles with a mean diameter of 150 μm were continuously fed into a fluidized bed with a diameter of 7.27 m and inventory of 80,140 kg. The particles were roasted at 900 °C in the fluidizing air with U_o = 0.6 m/s. The measured velocity of the gas and bed voidage at minimum fluidization conditions were 0.025 m/s and 0.5, respectively. The predictions of the newly developed model are compared with the data in Table 4, in terms of the conversion of reactants at two different feed rates of solid particles. From Table 4, the computed reactant conversions from both methods show close agreement; thereby provide another useful validation of the current formulation.

Two limiting reaction kinetics (VM and SCM) of $CuCl_2$ particles in the hydrolysis reaction were considered. The results are presented in terms of the conversion of reactants, inter-phase effectiveness factor and bed effectiveness, at various process parameters for a typical lab-scale fluidized bed reactor with a diameter of 2.66 cm and a height of 16 cm. The outcomes are given separately for VM and SCM cases using solution algorithms developed by Haseli et al. [24]. Then the predictions of these two limiting kinetic models are compared and discussed.

The predicted steam and $CuCl_2$ particle conversions at various superficial gas velocities and three typical bed inventories are shown in Fig. 2. The solid conversion increases with the fluidizing gas velocity, since the solid particles are more immersed with steam. On the other hand, however, the steam conversion decreases as its superficial velocity increases. For a certain quantity of bed inventory and constant particle feed rate, a higher superficial velocity means a higher gas flow rate, which consequently results in less conversion of steam. Furthermore, from Fig. 2, a higher bed inventory improves the conversion of both reactants. At given feed rates of reactants, the mean residence time, $\bar{t}$, increases as the bed inventory rises. Thus, the contact opportunity for both reactants increases.

Fig. 3 shows the variation of the inter-phase effectiveness factor with superficial velocity and bed inventory. Higher conversion of steam corresponds to the situation where the concentration of steam at the outlet stream and its concentration in the emulsion are accordingly lower. Thus, the inter-phase effectiveness factor is lower at the higher gas conversion, which results from a higher bed inventory and less superficial velocity, as discussed above in Fig. 2.

Further results involve the influences of various process parameters on the bed effectiveness, η_{bed}, defined in Section 2.3. Conversion of solid particles and steam is represented by this new parameter, indicating the net performance of the fluidized bed reactor. Fig. 4 shows the variation of η_{bed} versus superficial gas

Table 3
Comparison of predictions of the current method and the past data of Gómez-Barea et al. [25] for a zinc roaster in an industrial fluidized bed.

Parameter	Gómez-Barea et al. [25]	Current method
Na	0.76	0.883
α	1.35	1.355
X_g	0.74	0.736
$x_{c,b}$	0.99	0.997

Table 4
Comparison of predictions of the current model and the past data of Kunii and Levenspiel [23] for a zinc roaster in an industrial fluidized bed.

F_o (kg/s)	Parameter	Kunii and Levenspiel [23]	Current method
2	X_g	0.661	0.666
	$x_{c,b}$	0.991	0.999
2.5	X_g	0.808	0.833
	$x_{c,b}$	0.970	0.999

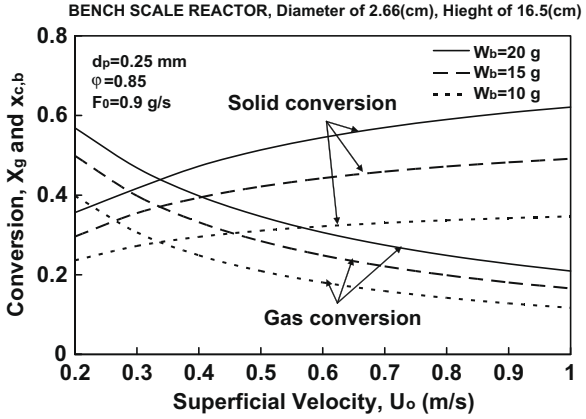

Fig. 2. Conversion of cupric chloride particles and steam for a typical range of superficial gas velocities at three bed inventories (Volumetric Model).

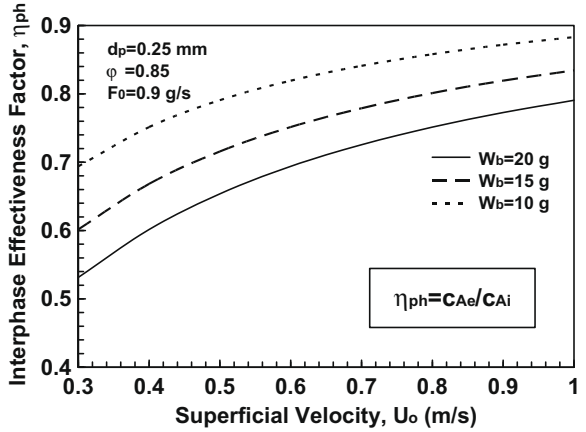

Fig. 3. Variation of inter-phase effectiveness factor, ηph, with superficial velocity at three bed inventories (Volumetric Model).

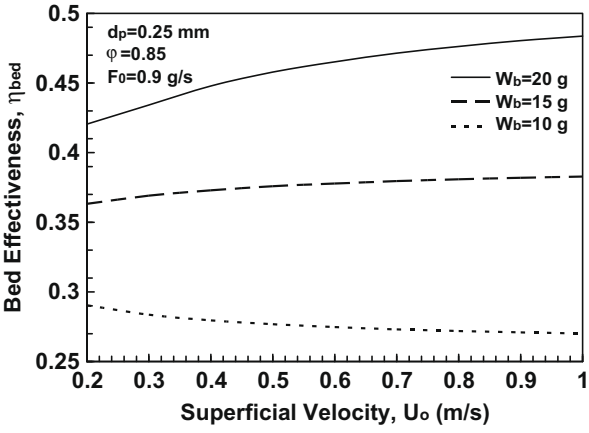

Fig. 4. Predicted bed effectiveness at various superficial velocities (Volumetric Model).

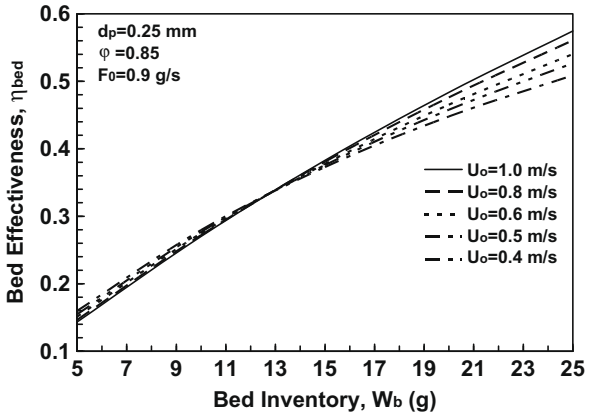

Fig. 5. Dependence of bed effectiveness on bed inventory (Volumetric Model).

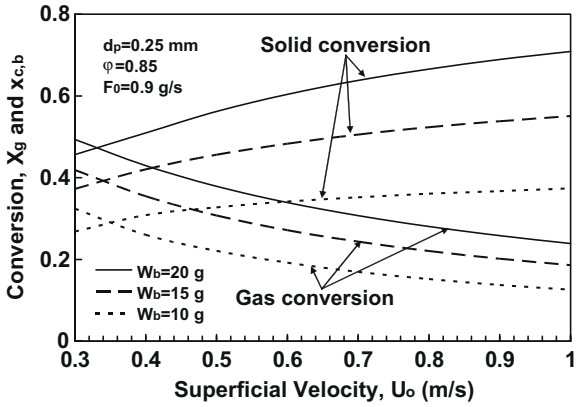

Fig. 7. Conversion of cupric chloride particles and steam for a typical range of superficial gas velocities at three bed inventories (Shrinking Core Model).

velocity at three bed inventories. From this figure, the effect of superficial velocity on η_{bed} depends on bed inventory. The reason for this trend can be explained based on the dependence of steam and particle conversions on superficial velocity, as described previously for Fig. 2. As the particle conversion increases, while conversion of steam decreases with superficial velocity, the interaction of these two trends will influence the value of bed effectiveness. This phenomenon is further investigated and the results are depicted in Fig. 5, where the bed effectiveness changes with bed inventory at a varying gas velocity. The graphs in Fig. 5 are divided into two regions. When the bed inventory exceeds 13 g, a higher velocity leads to a larger bed effectiveness. On the other hand, for a bed inventory of less than 13 g, a higher superficial velocity results in less bed effectiveness.

The influence of bed temperature, a key process parameter, on η_{bed} is illustrated in Fig. 6 at varying superficial velocities. This figure suggests that a lower bed temperature improves the performance of the process. When the bed temperature decreases, the conversion of cupric chloride particles rises, with no significant change in steam conversion. Similar results are obtained based on the Shrinking Core Model (SCM), as depicted in Figs. 7–11, in terms of the conversion of reactants and bed effectiveness. The only qualitative difference is seen in Fig. 10, which shows the effects of bed inventory on η_{bed} at various gas velocities. Unlike Fig. 5, at a bed inventory smaller than 12 g, the superficial velocity does not have a significant effect on η_{bed}. On the other hand, as the

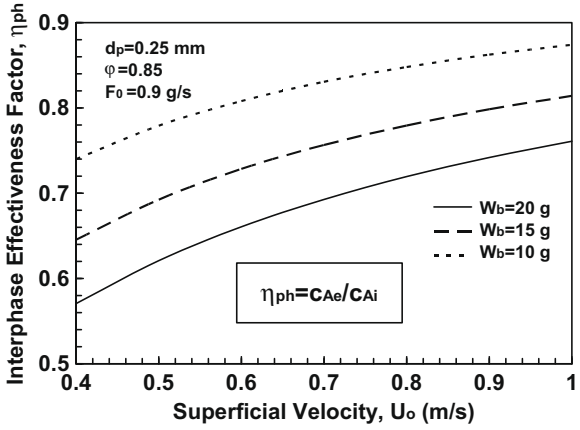

Fig. 8. Variation of inter-phase effectiveness factor with superficial velocity at three bed inventories (Shrinking Core Model).

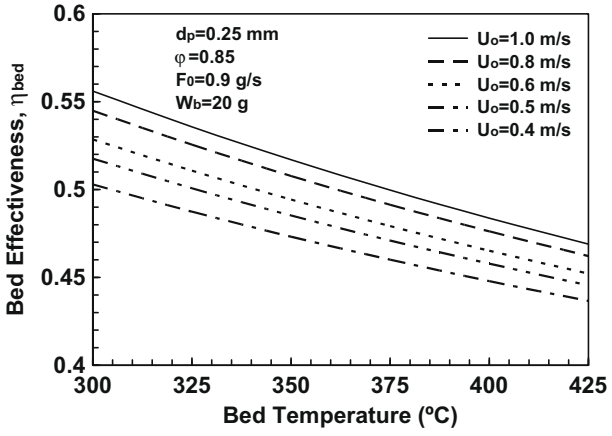

Fig. 6. Dependence of bed effectiveness on bed temperature at different superficial velocities (Volumetric Model).

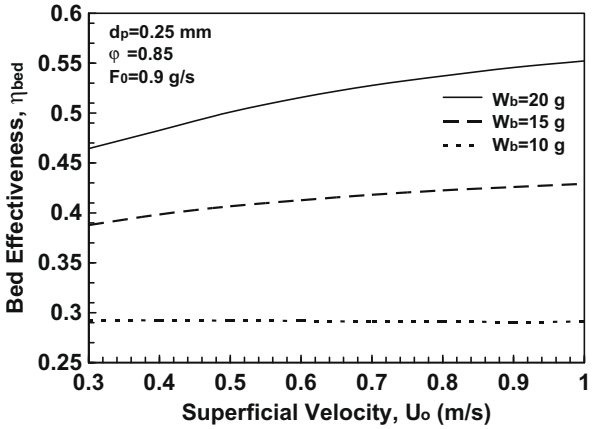

Fig. 9. Predicted bed effectiveness at various superficial velocities (Shrinking Core Model).

inventory exceeds 12 g, a higher velocity results in higher bed effectiveness.

The predictions of the two kinetic models are compared herein. The computed reactant conversions and inter-phase effectiveness factor, based on VM and SCM, are shown in Figs. 12 and 13, respectively, under identical process conditions. Figure 12 indicates that if the kinetics of solids follows the SCM, the conversion of both

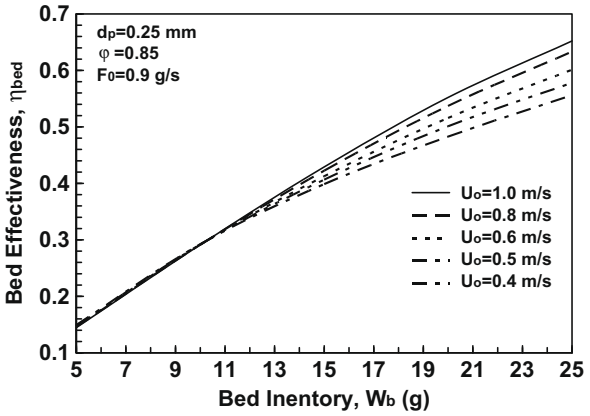

Fig. 10. Dependence of bed effectiveness on bed inventory (Shrinking Core Model).

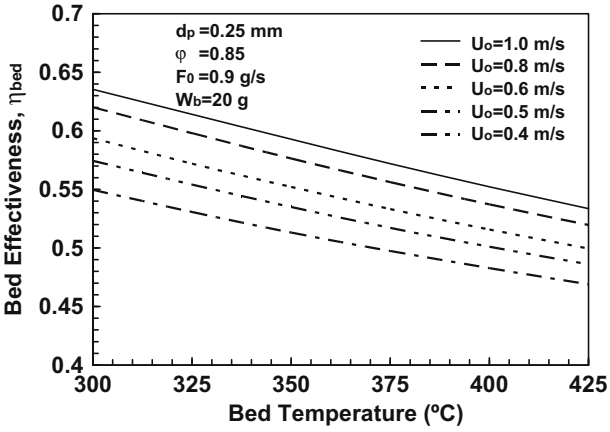

Fig. 11. Dependence of bed effectiveness on bed temperature at different superficial velocities (Shrinking Core Model).

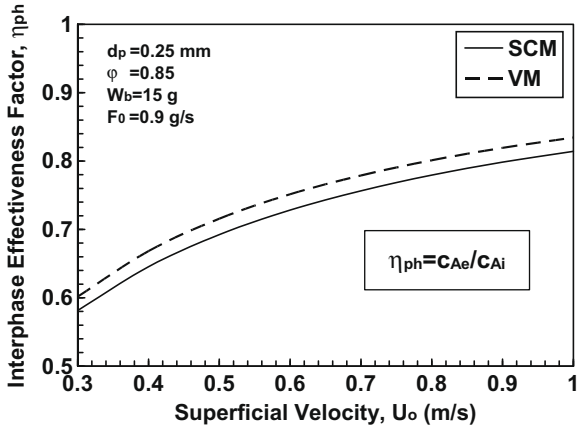

Fig. 13. Comparison of predictions of SCM and VM in terms of the inter-phase effectiveness factor.

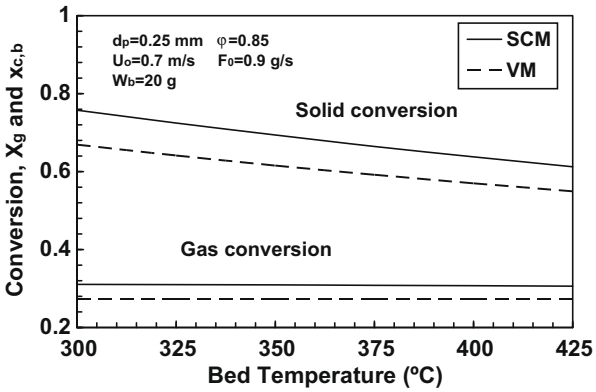

Fig. 14. Comparison of predictions of SCM and VM in terms of conversion of CuCl2 particles and steam versus bed temperature.

$CuCl_2$ particles and fluidizing steam would be higher than the prediction by VM. Further comparisons of kinetic models are made in Fig. 13, in terms of the inter-phase effectiveness factor, η_{ph}. From Fig. 13, the SCM prediction of η_{ph} is less than VM. The reason can be inferred from Fig. 12, where conversion of gaseous reactant is higher for the SCM, compared to VM. Thus, the mean concentration of steam in the emulsion becomes less for the case of SCM, and η_{ph} based on the SCM is lower than that of VM.

The influence of the bed temperature on conversion of $CuCl_2$ particles and steam is illustrated in Fig. 14, based on both SCM and VM for a certain process condition. An interesting result from this figure is that the reaction temperature affects the solid particle conversion, but it has no significant effect on conversion of the fluidizing gas. Fig. 14 suggests that lowering the reaction temperature improves the conversion of cupric chloride particles. At lower temperatures, the concentration of steam is higher and the kinetic coefficient is higher, since it is proportional to the concentration, as shown in Eq. 12. Hence, for a given quantity of solid inventory,

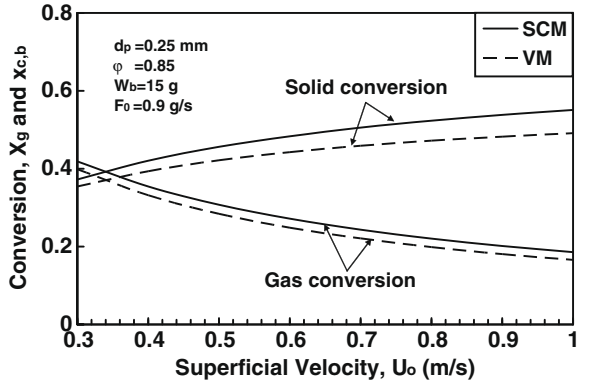

Fig. 12. Comparison of predictions of SCM and VM in terms of reactant conversions.

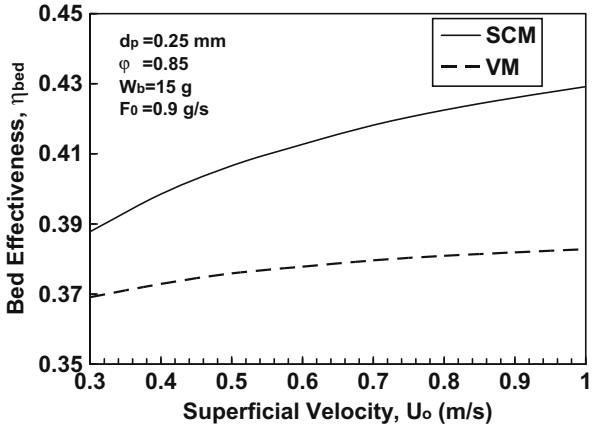

Fig. 15. Comparison of predictions of SCM and VM in terms of the bed effectiveness versus superficial velocity.

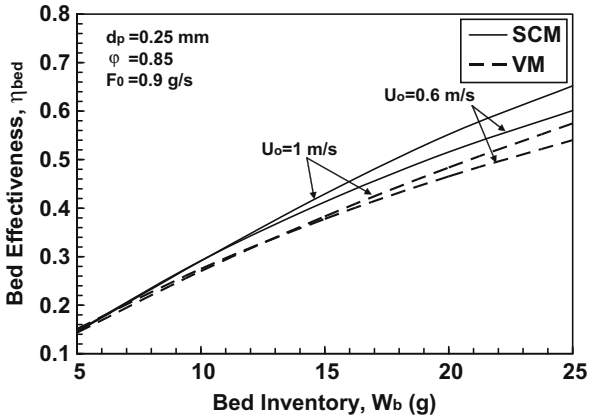

Fig. 16. Comparison of predictions of SCM and VM in terms of the bed effectiveness versus bed inventory.

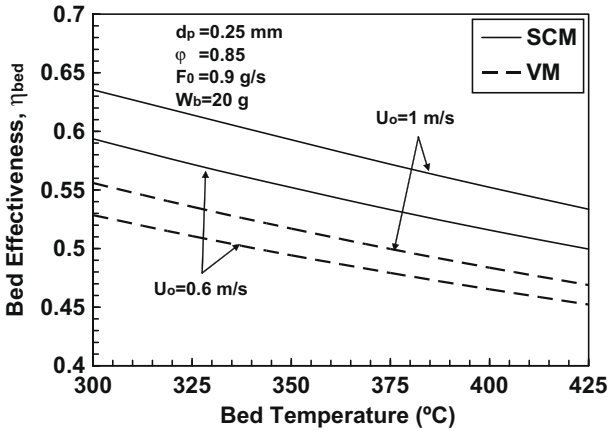

Fig. 17. Comparison of predictions of SCM and VM in terms of the bed effectiveness versus bed temperature.

there is more opportunity for particles to be immersed by the fluidizing gas stream.

The bed effectiveness profiles, predicted by SCM and VM, are compared at varying superficial velocities, bed inventories and bed temperatures in Figs. 15–17, respectively. In these figures, the profiles of SCM are higher than those of VM. In Fig. 15, at higher gas velocities (almost greater than 0.6 m/s), the bed effectiveness based on the VM is approximately independent of velocity, whereas the SCM profile still increases at higher velocities. Moreover, from Fig. 16, at a smaller bed inventory (less than 10 g), the prediction of both models is almost the same. As discussed previously, a lower bed temperature improves the bed effectiveness, due to the enhanced conversion of solid particles. An illustrative example of SCM and VM predictions of η_{bed} versus temperature is depicted in Fig. 17. Based on discussions presented previously, the higher prediction of η_{bed} by SCM compared to VM occurs because SCM predicts the conversion of both reactants is higher than those computed by VM at a given process condition.

4. Conclusions

In this paper, a parametric study was carried out for the transport phenomena in a hydrolysis reaction of cupric chloride particles and superheated steam in a lab-scale fluidized bed reactor, as part of the copper–chlorine (Cu–Cl) thermochemical cycle of hydrogen production. Both cupric chloride particles and steam participate in the chemical reaction. The method of Gómez-Barea and co-workers [25] was extended to analyze the Non-Catalytic Gas–Solid Reaction. Due to the lack of experimental data of hydrodynamics and chemistry of the reaction to define the kinetics of the particle reaction, the Volumetric Model (VM) and Shrinking Core Model (SCM) were used as limiting cases in this paper. Validation of the newly developed method was performed by comparing the predicted process parameters with past data of Gómez-Barea et al. [25], as well as computed values based on the method of Kunii and Levenspiel [23] for zinc roasting processes. Then, full simulations were performed for each kinetic model for the hydrolysis reaction of cupric chloride particles. The computed outcomes indicate that SCM quantitatively made a greater conversion of gas and particles and bed effectiveness compared to VM. As the superficial steam velocity increases, the conversion of solid particles improves, but conversion of steam decreases. When the bed inventory is higher, both reacting species conversions increase. As confirmed by both kinetic models, cupric chloride particle conversions are increased by lowering the bed temperature, whereas steam conversion shows no significant change. Furthermore, a new parameter called the "bed effectiveness", defined as the fraction of total reactant moles converted to products, is increased by raising the superficial velocity, or bed inventory, or lowering the bed temperature. The findings of this paper will have valuable utility for equipment design and scale-up of the copper–chlorine thermochemical cycle of nuclear-based hydrogen production.

Acknowledgements

The authors gratefully acknowledge the support provided by Atomic Energy of Canada Limited (particularly Dr. S. Suppiah and Dr. A. Miller) and the Ontario Research Excellence Fund. The first author acknowledges personal communication with Dr. Alberto Gómez-Barea, who provided valuable assistance through his past articles.

References

[1] M.A. Rosen, G.F. Naterer, R. Sadhankar, S. Suppiah, Nuclear-based hydrogen production with a thermochemical copper–chlorine cycle and supercritical water reactor, Canadian Hydrogen Association Workshop, Quebec, 2006.
[2] B. Yildiz, M.S. Kazimi, Efficiency of hydrogen production systems using alternative nuclear energy technologies, Int. J. Hydrogen Energy 31 (2006) 77–92.
[3] C.W. Forsberg, Hydrogen, nuclear energy, and the advanced high-temperature reactor, Int. J. Hydrogen Energy 28 (2003) 1073–1081.
[4] G.F. Naterer, Heat Transfer in Single and Multiphase Systems, first ed., CRC Press, Boca Raton, FL, 2002.
[5] M. Nomura, S. Fujiwara, K. Ikenoya, S. Kasahara, H. Nakajima, S. Kubo, G.I. Hwang, H.S. Choi, K. Onuki, Application of an electrochemical membrane reactor to the thermochemical water splitting IS process for hydrogen production, J. Membrane Sci. 240 (2004) 221–226.
[6] S. Kasahara, G.J. Hwang, H. Nakajima, H.S. Choi, K. Onuki, M. Nomura, Effects of process parameters of the IS process on total thermal efficiency to produce hydrogen from water, J. Chem. Eng. Jpn. 36 (7) (2003) 887–899.
[7] S. Kasahara, S. Kubo, K. Onuki, M. Nomura, Thermal efficiency evaluation of HI synthesis/concentration procedures in the thermochemical water splitting IS process, Int. J. Hydrogen Energy 29 (2004) 579–587.
[8] S. Kasahara, S. Kubo, R. Hino, K. Onuki, M. Nomura, S. Nakao, Flowsheet study of the thermochemical water-splitting iodine–sulfur process for effective hydrogen production, International Journal of Hydrogen Energy 32 (2007) 489–496.
[9] C.W. Forsberg, P.F. Peterson, P.S. Pickard, Molten-salt-cooled advanced high-temperature reactor for production of hydrogen and electricity, Nucl. Technol. 144 (2003) 289–302.
[10] W.A. Summers, M.B. Gorensek, Nuclear hydrogen production based on the hybrid sulfur thermochemical process, in: Proceedings of the International Congress on Advances in Nuclear Power Plants 06, Reno, NV, 2006, pp. 2254–2256.
[11] M.A. Lewis, J.G. Masin, R.B. Vilim, Development of the low temperature Cu–Cl thermochemical cycle, in: Proceedings of the International Congress on Advances in Nuclear Power Plants 05, Seoul, 2005.

[12] R.R. Sadhankar, J. Li, H. Li, D.K. Ryland, S. Suppiah, Future hydrogen production using nuclear reactors, in: Proceedings of the Climate Change Technology Conference, Engineering Institute of Canada, Ottawa, 2006.
[13] M. Lewis, Cu–Cl cycle R&D, Workshop on Thermochemical Nuclear-Based Hydrogen Production, UOIT, Oshawa, Ontario, 2007.
[14] M. Serban, M.A. Lewis, J.K. Basco, Kinetic study of the hydrogen and oxygen production reactions in the copper-chloride thermochemical cycle, AIChE National Meeting, New Orleans, LA, 2004.
[15] Y. Haseli, I. Dincer, G. F. Naterer, Hydrodynamics of cupric chloride hydrolysis in a fluidized bed for nuclear hydrogen production, in: Proceedings of the 29th Conference of the Canadian Nuclear Society, Toronto, 2008.
[16] G.F. Naterer, Multiphase flow with impinging droplets and airstream interaction at a moving gas/solid interface, Int. J. Multiphase Flow 28 (3) (2002) 451–477.
[17] L. Lin, R. Ponnappan, Heat transfer characteristics of spray cooling in a closed loop, Int. J. Heat Mass Transfer 46 (20) (2003) 3737–3746.
[18] G. Castanet, P. Lavieille, L. Lemoine, M. Lebouché, A. Atthasit, Y. Biscos, G. Lavergne, Energetic budget on an evaporating monodisperse droplet stream using combined optical methods: evaluation of the convective heat transfer, Int. J. Heat Mass Transfer 45 (25) (2002) 5053–5067.
[19] R.T. Imaoka, W.A. Sirignano, Transient vaporization and burning in dense droplet arrays, Int. J. Heat Mass Transfer 48 (21–22) (2005) 4354–4366.
[20] S. Hohmann, U. Renz, Numerical simulation of fuel sprays at high ambient pressure: the influence of real gas effects and gas solubility on droplet vaporization, Int. J. Heat Mass Transfer 46 (16) (2003) 3017–3028.
[21] G.F. Naterer, C.D. Tokarz, J. Avsec, Fuel cell entropy production with ohmic heating and diffusive polarization, Int. J. Heat Mass Transfer 49 (15) (2006) 2673–2683.
[22] P. Basu, Combustion and Gasification in Fluidized Beds, Taylor and Francis Group LLC, Boca Raton, FL, 2006.
[23] D. Kunii, O. Levenspiel, Fluidization Engineering, second ed., Butterworth, Heinemann, London, 1991.
[24] Y. Haseli, I. Dincer, G.F. Naterer, Hydrodynamic gas-solid model of cupric chloride particles reacting with superheated steam for thermochemical hydrogen production, Chem. Eng. Sci. 63 (2008) 4596–4604.
[25] A. Gómez-Barea, B. Leckner, D. Santana, P. Ollero, Gas–solid conversion in fluidized bed reactors, Chem. Eng. J. 141 (2008) 151–168.
[26] W.C. Yang, Handbook of Fluidization and Fluid-Particle Systems, second ed., Taylor and Francis, Group LLC, New York, 2003.